JOURNAL OF MATERIALS SCIENCE 27 (1992) 4717–4725

Characterization of grain-boundary configuration and fracture surface roughness by fractal geometry and creep-rupture properties of metallic materials

MANABU TANAKA
Department of Mechanical Engineering, Mining College, Akita University, 1-1 Tegatagakuen-cho, Akita 010, Japan

Grain-boundary configuration in heat-treated specimens and fracture surface roughness in creep-ruptured specimens of several kinds of metallic material were quantitatively evaluated on the basis of fractal geometry. Correlations between the fractal dimension of grain boundary, that of fracture surface profile, the creep-rupture properties and the fracture mechanisms of the alloys are discussed. In heat-resistant alloys, the fractal dimension of a nominally serrated grain boundary was always larger than that of a straight grain boundary in the same alloy. The relative importance of the ruggedness of grain boundaries was estimated by the fractal dimension difference between these two grain boundaries. There was a quantitative relationship between the increase of the fractal dimension of the grain boundary and the improvement of rupture ductility and rupture strength owing to grain-boundary serration in the alloy. A similar correlation was also found between the increase in the fractal dimension of the fracture surface profile and the improvement of the creep-rupture properties, since in some cases the fractal dimension of the fracture surface profile was correlated with that of the grain boundary. Both grain boundary and fracture surface profile were assumed to exhibit a fractal nature between one grain boundary length (upper bound) and an interatomic spacing (lower bound). In carbon steels with ferrite–pearlite structure, according to the increase in pearlite volume fraction, the rupture ductility decreased and the fracture mechanism changed from transgranular fracture in pure iron and low-carbon steels to intergranular fracture at ferrite–pearlite grain boundaries in medium-carbon steels, and further to intergranular fracture at pearlite grain boundaries in high-carbon steels. The correspondence between the fractal dimension of the grain boundary and that of the fracture surface was confirmed in ruptured specimens of ferrite–pearlite steels when the grain boundary was the fracture path.

1. Introduction

Mandelbrot *et al.* [1] have revealed that there is a correlation between the fractal dimension of the fracture surface roughness and the energy absorbed in impact-loaded and fractured specimens. They also pointed out the correlation between the fracture profile and the microstructure of a specimen. Similar investigations were also made by other investigators [2–9]. Hornbogen [2] analysed the deformation of grains by cold work using the fractal dimension of a grain boundary. Kleiser and Boček [5] examined the self-similarity of the slip-line patterns in Cu and Co.

In polycrystalline heat-resistant alloys, strengthening of grain boundaries by modification of the grain-boundary configuration is one of the most effective methods to improve high-temperature strength. It has been reported in austenitic heat-resisting steels [10, 11] that both initiation and growth of grain-boundary cracks are retarded by serrated grain boundaries in high-temperature creep. The strengthening by serrated grain boundaries is principally attributed to the retardation of grain-boundary sliding [10], the decrease in stress concentration at grain-boundary triple junctions [12–16], the crack deflection which results in a decreased stress intensity of a grain-boundary crack leading to the retardation of crack growth [17–19], the lengthening of the fracture path [19], and the occurrence of ductile grain-boundary fracture [15, 20] . All these strengthening effects can be correlated with the ruggedness of serrated grain boundaries. However, the configuration of actual serrated grain boundaries is too complicated to be quantitatively characterized, although it has been expressed by the average segment length [16] or the wavelength and amplitude of serrated grain boundaries [21] in some cases.

A previous study [22] revealed that there is a certain self-similarity in serrated grain boundaries in

0022–2461

TABLE I Chemical composition of the heat-resistant alloys used for fractal analysis or creep-rupture experiments in this study

Alloy	Composition (wt %)														
	C	N	Cr	Ni	Co	Fe	Mn	Al	Ti	W	Nb	Mo	Si	S	P
21Cr–4Ni–9Mn steel	0.54	0.39	21.10	4.07	–	Bal.	9.74	–	–	–	–	–	0.19	0.008	0.017
HS-21	0.27	B 0.003	26.71	2.37	Bal.	0.09	0.64	–	–	–	–	5.42	0.59	0.007	< 0.005
L-605	0.07	–	19.82	9.83	Bal.	2.22	1.46	–	–	14.37	–	–	0.19	0.002	< 0.005
Inconel X-750	0.06	–	15.03	Ni (+Co) 71.80		7.48	0.31	1.26	2.43	–	Nb + Ta 1.01	Cu 0.13	0.26	0.001	0.007
Inconel 751	0.09	–	16.07	Bal.	–	5.74	0.53	1.10	2.05	–	Nb + Ta 1.18	Cu 0.05	0.20	0.007	–

TABLE II Heat-treatments, grain-boundary configuration, grain diameter and matrix hardness of heat-resistant alloys

Alloy	Type of grain boundary	Heat treatment[a]	Grain diameter (μm)	Matrix hardness (H_V, load 4.9 N)
21Cr–4Ni–9Mn steel	Straight	1473 K–3.6 ks → W.Q. + 973 K–108 ks → A.C. + 1273 K–108 ks → A.C.	99	320
	Serrated	1473 K–3.6 ks–F.C. → 1303 K → W.Q. + 1023 K–108 ks → A.C. + 1273 K–10.8 ks → A.C.	99	320
HS-21	Straight	1523 K–3.6 ks → W.Q.	130	315
	Serrated	1523 K–3.6 ks–F.C. → 1323 K → W.Q.	130	317
L-605	Straight	1473 K–7.2 ks → W.Q.	255	253
	Serrated	1473 K–3.6 ks–F.C. → 1323 K–72 ks → W.Q.	260	249
Inconel X-750	Straight	1423 K–7.2 ks → W.Q.	108	201
	Serrated	1423 K–7.2 ks–F.C. → 1323 K–21.6 ks → W.Q.	125	190
Inconel 751	Straight	1473 K–7.2 ks → W.Q. + 1023 K–86.4 ks → A.C.	165	330
	Serrated	1473 K–7.2 ks–D.A. → 1173 K–21.6 ks → A.C. + 1023 K–86.4 ks → A.C.	165	312

[a] WQ: water-quenched, FC: furnace-cooled, AC: air-cooled, DA: directly aged.

commercial heat-resistant alloys, and that it would be possible to characterize quantitatively the ruggedness of serrated grain boundaries in terms of the concept of fractal geometry [23, 24]. It was also found that there is a relationship between the improvement of creep-rupture properties and the relative increase of the fractal dimension of the grain boundary owing to grain-boundary serration in these alloys. However, correlations between the grain-boundary configuration, the fracture surface roughness, the creep-rupture properties and the fracture mechanism have not quantitatively discussed.

In this study, the fractal dimension of the grain boundary in heat-treated specimens and that of the fracture surface profile in creep-ruptured specimens were estimated on several heat-resistant alloys and carbon steels. Correlations between these fractal dimensions, the creep-rupture properties and the fracture mechanisms in these materials are then discussed. The fractal dimensions were obtained by the vertical section method [7–9] in this study, since this method was considered to be suitable for evaluating both the grain-boundary configuration and the fracture surface roughness. Experimental techniques to estimate the fractal dimension of the grain boundary and that of the fracture surface profile were also examined.

2. Measurements of fractal dimension in alloys

2.1. Materials

Table I shows the chemical composition of the heat-resistant alloys of iron base, nickel base and cobalt base used for the fractal analysis or creep-rupture experiments in this study. Table II shows the heat treatments, the grain-boundary configuration, the grain diameter and the matrix hardness of the heat-resistant alloys. The experimental results on Inconel 751 alloy were taken from Yoshiba *et al.* [25]. Table III shows the chemical composition of carbon steels

TABLE III Chemical composition and volume fraction of pearlite in carbon steels with ferrite–pearlite structure

Steel	Chemical composition (wt %)					Volume fraction of pearlite
	C	Si	Mn	P	S	
Pure iron	0.03	0.19	0.28	0.015	0.011	0
S10C	0.13	0.29	0.55	0.016	0.017	0.169
S20C	0.22	0.22	0.45	0.016	0.018	0.286
S40C	0.41	0.20	0.77	0.013	0.020	0.532
S50C	0.54	0.20	0.76	0.010	0.017	0.701
S70C	0.72	0.21	0.48	0.011	0.011	0.935
S80C	0.83	0.21	0.48	0.011	0.004	1.0

TABLE IV Fractal dimension of grain boundary obtained by Equation 2 or Equation 3 on heat-treated specimens of several heat-resistant alloys

Alloy	Equation used	Type of grain boundary		Difference, ΔD
		Serrated	Straight	
21Cr–4Ni–9Mn steel	2	1.142 (1.172)	1.020 (1.035)	0.122 (0.137)
	3	1.252	1.108	0.144
L-605	2	1.097	1.008	0.089
	3	1.205	1.080	0.125
HS-21	2	1.228	1.016	0.212
	3	1.324	1.086	0.238
Inconel X-750	2	1.048	1.012	0.036
	3	1.160	1.026	0.134
Inconel 751	2	1.155 (1.162)	1.049 (1.066)	0.106 (0.096)
	3	1.290	1.112	0.178

used for similar analysis. The specimens of these carbon steels were air-cooled to 973 K after heating for 3.6 or 7.2 ks in the temperature range from 1323 to 1423 K and then furnace-cooled from 973 K to room temperature to develop ferrite–pearlite structure. The grain diameter of the steels was in the range from 72 to 82 μm. Creep-rupture experiments were carried out by loading a dead weight to a specimen with a single lever-type creep-rupture apparatus in the temperature range from 873 to 1422 K after 3.6 ks (Inconel X-750 alloy) or 10.8 ks (other alloys) holding at each test temperature.

2.2. Methods for evaluation of fractal dimension

Several experimental techniques to estimate the fractal dimension have been proposed so far [1–3, 7–9], but the vertical section method [7–9] is considered to be suitable for the measurement of both the fractal dimension of grain boundary and that of the fracture surface profile, while the slit island method is used for the evaluation of fracture surface roughness [1, 8]. Grain boundaries and fracture surface profiles in specimens were observed by optical or scanning electron microscopy at various magnifications up to about 10 000 ×. About five grain boundaries or a fracture surface profile of about five-grain-boundary length were examined for each photograph of the polished and etched surface of heat-treated specimens or that of the longitudinally sectioned plane of ruptured specimens.

The fractal dimension, D, relates the length of the grain boundary or that of the fracture surface profile, L, to the unit length of a scale, s (the opening of the dividers used for measurement) by the relation [6, 7]

$$L = L_0 s^{1-D} \quad (1)$$

where L_0 is a constant. According to Haussdorf's definition [24], there is also a relationship between the diameter of circles, s, covering grain boundaries or fracture surface profiles, and the number of the circles, N, such that [24, 26]

$$N = M_0 s^{-D} \quad (2)$$

where M_0 is a constant. Further, the size of square grids, r, can be correlated with the number of grids intersected by grain boundaries or fracture surface profiles, N_r, through the equation [24]

$$N_r = N_0 r^{-D} \quad (3)$$

where N_0 is a constant. It was found in this study that Equation 1 gives the same value of the fractal dimension of the grain boundary or that of the fracture surface profile as Equation 2. Therefore, the analysis of grain boundaries and fracture surface profiles was made on the basis of Equations 2 and 3.

3. Fractal dimensions of grain boundary and fracture surface profile

3.1. Fractal dimension of grain boundary in heat-treated specimens

Table IV shows the fractal dimensions estimated by Equation 2 or 3 of serrated and straight grain boundaries in heat-treated specimens of several heat-resistant alloys. The fractal dimension data by Equation 3 were taken from the previous study [22]. Nominally serrated grain boundaries have the larger values of the fractal dimension than straight grain boundaries, although the fractal dimension difference between these two grain boundaries (ΔD) depends on the alloy. Some of these values by Equation 2 were estimated along the centre of grain-boundary precipitates and are somewhat smaller than the values measured along the irregular contour of the grain-boundary precipitates (the values in parenthesis). The fractal dimension estimated by Equation 3 is always larger than that obtained by Equation 2, probably because the method using square grids measures both sides of precipitate–matrix interfaces on grain boundaries, while the results of analysis by Equation 3 tend to give larger values of the fractal dimension compared with those by Equation 2.

Fig. 1 shows serrated and straight grain boundaries in heat-treated specimens of 21Cr–4Ni–9Mn steel. $M_{23}C_6$ carbide particles are visible on grain boundaries and in the grains in both the specimen with serrated grain boundaries (Fig. 1a) and the one with

TABLE V Fractal dimension of grain boundary in heat-treated specimens and that of fracture surface profile in ruptured specimens of heat-resistant alloys

Alloy	Condition[a]	Type of grain boundary		Difference, ΔD
		Serrated	Straight	
21Cr–4Ni–9Mn steel	As heat-treated	1.142	1.020	0.122
	Fracture surface	1.155	1.088	0.067
L-605	Held for 10.8 ks at 1089 K	1.077	1.041	0.036
	Fracture surface (1089 K, 118 MPa)	1.155	1.124	0.031
	Grain boundary in ruptured specimen	1.101	1.092	0.009
	Aged for 1080 ks at 1273 K	1.063	1.033	0.030
	Fracture surface (1089 K, 137 MPa)	1.138	1.120	0.018
	Fracture surface (1311 K, 29.4 MPa)	1.186	1.110	0.076
HS-21	Held for 10.8 ks at 1089 K	1.187	1.023	0.164
	Fracture surface (1089 K, 137 MPa)	1.172	1.043	0.129
	Grain boundary in ruptured specimen	1.170	1.039	0.131
	Held for 10.8 ks at 1422 K	1.145	1.071	0.074
	Fracture surface (1422 K, 19.6 MPa)	1.116	1.122	− 0.006
	Grain boundary in ruptured specimen	1.214	1.193	0.021
Inconel X-750	Held for 3.6 ks at 973 K	1.074	1.032	0.042
	Fracture surface (973 K, 29.4 MPa)	1.087	1.040	0.047
	Grain boundary in ruptured specimen	1.093	1.056	0.037
Inconel 751	As heat-treated	1.155	1.049	0.106
	Fracture surface	–	–	–

[a] Conditions of creep-rupture experiments are shown in parenthesis.

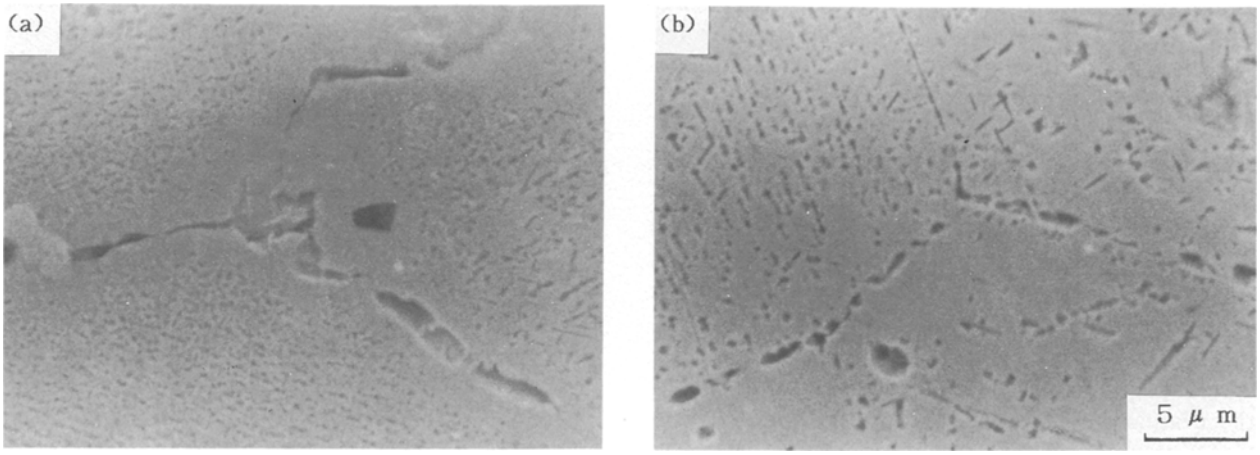

Figure 1 Grain-boundary configurations in heat-treated specimens of 21Cr–4Ni–9Mn steel: (a) serrated grain boundaries, (b) straight grain boundaries.

straight grain boundaries (Fig. 1b) [10]. Grain-boundary precipitates usually lie on the habit plane of the austenite matrix and only one side of a precipitate–matrix interface is a grain boundary, although it is difficult by optical or scanning electron microscopy to determine on which side of the interface a real grain boundary is. Therefore, the fractal dimension of grain boundary was measured using Equation 2 along the centre of the grain-boundary precipitates in this study.

3.2. Relation between fractal dimension of grain boundary and that of fracture surface profile

Table V shows the fractal dimension data estimated by Equation 2 of grain boundaries in heat-treated specimens and of fracture surface profiles in ruptured specimens of several heat-resistant alloys. Most specimens with serrated grain boundaries exhibited little or no change in the fractal dimension of grain boundary after high-temperature ageing or holding at each test temperature, except specimens of HS-21 alloy held for 10.8 ks at 1422 K. The fractal dimension of the grain boundary in specimens with straight grain boundaries increased after high-temperature ageing or holding at test temperatures because of the occurrence of grain-boundary precipitates [22]. However, prolonged exposure at high temperatures led to the coarsening or agglomeration of grain-boundary precipitates to minimize increases of the incoherent boundary area, resulting in a decrease of the fractal dimension of the grain boundary.

The fractal dimension of the fracture surface profile of a specimen with serrated grain boundaries is also larger than that of a specimen with straight grain boundaries. The fractal dimension of the fracture surface profile is almost the same as that of the grain boundary in 21Cr–4Ni–9Mn steel, Inconel 750 alloy and HS-21 alloy (ruptured under a stress of 137 MPa at 1089 K). Fig. 2 shows a fractal plot by Equation 2 of grain boundaries and fracture surface profiles in specimens with serrated grain boundaries of 21Cr–4Ni–9Mn steel. The fractal dimension of the fracture surface profile is close to that of the grain boundary. The results of regression analysis gave large values of the correlation factor R (more than 0.9995 in both cases). Both grain boundary and fracture surface profile are considered to exhibit a fractal nature between one-grain-boundary length (upper bound) and an atomic spacing (lower bound).

In L-605 alloy, the fractal dimension of the fracture surface profile is somewhat larger than that of the grain boundary in both specimens with serrated grain boundaries and those with straight grain boundaries. Fig. 3 shows the microstructures of specimens aged for 1080 ks at 1273 K and the fracture surface profiles of specimens ruptured under a stress of 137 MPa at 1089 K in L-605 alloy. Both grain-boundary and matrix precipitates of tungsten solid solution and M_6C carbide were detected in the specimen with serrated grain boundaries (Fig. 3a and b) and the one with straight grain boundaries (Fig. 3c and d) [27, 28]. Large local deformation can be observed in both the specimen with serrated grain boundaries and the one with straight grain boundaries (Fig. 3e and f) compared with the undeformed specimens (Fig. 3a and c).

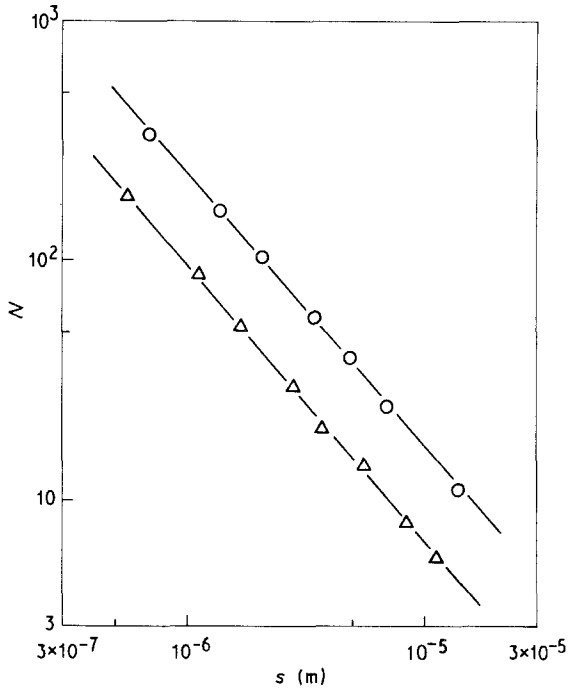

Figure 2 Fractal plot by Equation 2 of (○) grain boundaries ($D = 1.142$, $R = -0.9995$) and (△) fracture surface profiles ($D = 1.155$, $R = -0.9997$) in specimen with serrated grain boundaries of 21Cr–4Ni–9Mn steel.

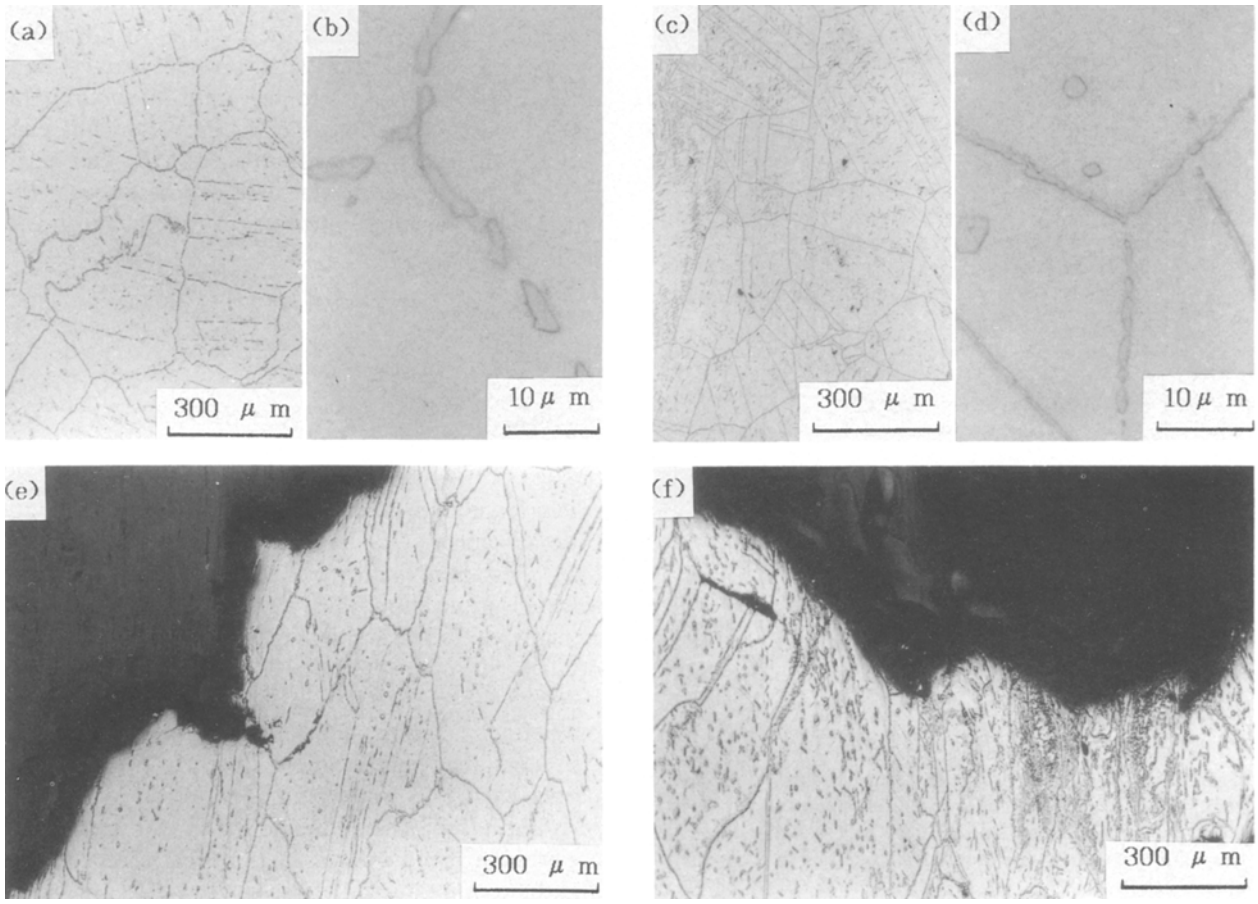

Figure 3 Microstructures of specimens aged for 1080 ks at 1273 K and fracture surface profiles of specimens ruptured under a stress of 137 MPa at 1089 K in L-605 alloy: (a, b) heat-treated specimen with serrated grain boundaries; (c, d) heat-treated specimen with straight grain boundaries; (e) ruptured specimen with serrated grain boundaries; (f) ruptured specimen with straight grain boundaries.

As Hornbogen pointed out [2], the fractal dimension of the grain boundary increases with plastic deformation of the grains. Larger creep deformation to rupture may lead to larger values of the fractal dimension of the fracture surface profile, since L-605 alloy has a large rupture ductility [27, 28] compared with other alloys in this study (e.g. [10, 22, 25]). Grain-boundary fracture may occur along the incoherent interface between grain-boundary precipitates and matrix. This implies that the fractal dimension of the fracture surface profile is generally somewhat larger than that of the grain boundary measured along the centre of grain-boundary precipitates, but the difference between these fractal dimensions in the present case is too large to be explained in this way.

On the other hand, in specimens of HS-21 alloy held for 10.8 ks and creep-ruptured at 1422 K (stress 19.6 MPa), the fractal dimension of the fracture surface profile is much the same in both the specimen with serrated grain boundaries and the one with straight grain boundaries. The fractal dimension of the fracture surface profile is smaller than that of the grain boundary in the ruptured specimens. The fractal dimension of the grain boundary is larger in the ruptured specimens than in the 10.8 ks-held specimens for both serrated and straight grain boundaries. As deduced from these values of the fractal dimension of the grain boundary, grain-boundary migration occurred during creep at 1422 K and this caused the increase of the fractal dimension of the grain boundary in these specimens. However, enhanced oxidation and surface diffusion at this temperature may also promote the smoothing of fracture surfaces in a very short period and may lead to a decrease of the fractal dimension of a fracture surface profile. Thus, there is a correlation between the fractal dimension of the grain boundary and that of the fracture surface profile in some cases, but the former value does not always correspond to the latter one.

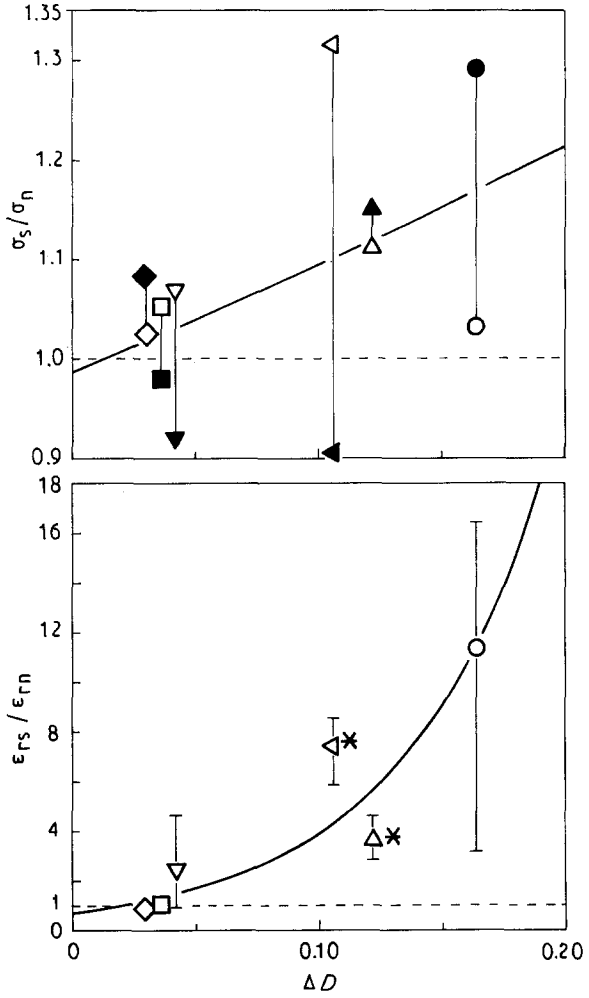

Figure 4 Relationship between increase of fractal dimension of grain boundary (ΔD) and improvement of creep-rupture properties owing to grain-boundary serration in heat-resistant alloys (test temperature shown in parenthesis; filled symbols 36 ks rupture life, open symbols 3600 ks). (●, ○) HS-21 (1089 K); (■, □) L-605 (1089 K); (◆, ◇) L-605 aged for 1080 ks at 1273 K (1089 K); (▲, △) 21Cr–4Ni–9Mn steel (973 K); (▼, ▽) Inconel X-750 (973 K); (◀, ◁) Inconel 751 (1073 K) (Yoshiba *et al.* [25]). Symbols with star refer to elongation tests.

3.3. Relations between fractal dimensions of grain boundary and fracture surface and creep-rupture properties

Fig. 4 shows the relationship between the increase of the fractal dimension of the grain boundary, ΔD, and the improvements of the creep-rupture properties owing to grain-boundary serration in heat-resistant alloys. The values of the fractal dimension and the pre-loading conditions of specimens are those listed in Table V. Effects of 10.8 ks holding at the test temperature are considered to be negligible in 21Cr–4Ni–9Mn steel and high-temperature aged L-605 alloy, and are therefore ignored in those alloys. Both the rupture strength ratio (σ_s/σ_n) and the rupture ductility ratio ($\varepsilon_{rs}/\varepsilon_{rn}$) of the specimen with serrated grain boundaries to the one with straight grain boundaries increased with increasing fractal dimension difference between these two grain boundaries, ΔD. The mean value of these experimental data can be fitted to the following exponential functions of the fractal dimension difference, ΔD:

$$\ln(\sigma_s/\sigma_n) = -0.01312 + 1.034\,\Delta D \quad (R = 0.9257) \tag{4}$$

$$\ln(\varepsilon_{rs}/\varepsilon_{rn}) = -0.3358 + 16.98\,\Delta D \quad (R = 0.9115) \tag{5}$$

where R is the correlation factor. The rupture strength ratio in some alloys is less than unity at short rupture lives. This may indicate that the strengthening by serrated grain boundaries is not so effective if sufficient precipitation hardening in the grains does not occur [15].

Fig. 5 shows the relationship between the increase of the fractal dimension of the fracture surface profile, ΔD, and the improvement of creep-rupture properties owing to grain-boundary serration in heat-resistant alloys. The values of the fractal dimensions are listed in Table V. Both the rupture life ratio (t_{rs}/t_{rn}) and the rupture ductility ratio ($\varepsilon_{rs}/\varepsilon_{rn}$) of the specimen with serrated grain boundaries to the one with straight grain boundaries increase with increasing fractal dimension difference of fracture surface profile, ΔD,

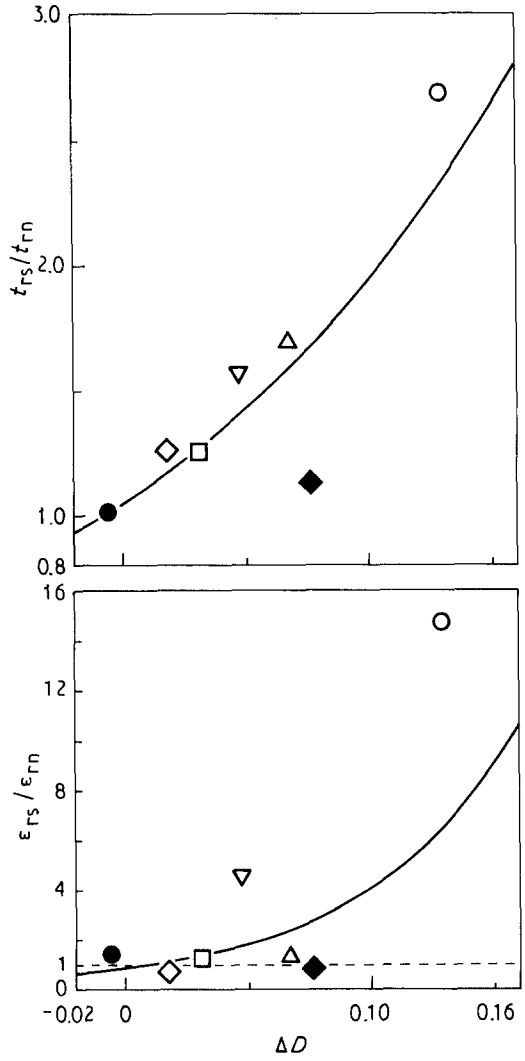

Figure 5 Relationship between fractal dimension difference of fracture surface profile (ΔD) and improvement of creep-rupture properties in heat-resistant alloys (test conditions shown in parenthesis). (○) HS-21 (1089 K, 137 MPa); (●) HS-21 (1422 K, 19.6 MPa); (□) L-605 (1089 K, 118 MPa); (◇) L-605 aged for 1080 ks at 1273 K (1089 K, 137 MPa); (◆) L-605 aged for 1080 ks at 1273 K (1311 K, 29.4 MPa); (△) 21Cr–4Ni–9Mn steel (973 K, 196 MPa); (▽) Inconel X-750 (973 K, 294 MPa).

owing to serrated grain boundaries. Both experimental data were fitted to the following exponential functions of the fractal dimension difference, ΔD, although the improvement of creep-rupture properties is not so well correlated with the fractal dimension difference of fracture surface profile compared with that of grain boundary.

$$\ln(t_{rs}/t_{rn}) = 0.04507 + 6.179\,\Delta D \quad (R = 0.8298) \tag{6}$$

$$\ln(\varepsilon_{rs}/\varepsilon_{rn}) = -0.2144 + 16.12\,\Delta D \quad (R = 0.6488) \tag{7}$$

As shown in Equation 1 in section 2.2, the length of a grain boundary, L, is a function of the length of the scale, s, used for the measurement of the fractal dimension, D. As pointed out in the previous study [22], the improvement of creep-rupture properties is attributed to an increase of rupture ductility owing to grain-boundary serration, and the increase of the rupture ductility can be correlated with the increases in the ruggedness and the length of grain boundaries. Therefore, the rupture ductility ratio $\varepsilon_{rs}/\varepsilon_{rn}$ of the specimen with serrated grain boundaries to the one with straight grain boundaries is associated with the ratio of the grain-boundary length between these boundaries through the fractal dimension difference, ΔD:

$$\varepsilon_{rs}/\varepsilon_{rn} = F s^{-\Delta D} \tag{8}$$

where F is a constant, if other materials factors are the same in each alloy (Table II) [22]. The same relationship may exist between the fractal dimension difference of fracture surface profile and the rupture ductility. The rupture life, t_r, and the steady-state creep rate, $\dot{\varepsilon}_s$, of materials can be correlated by a Monkman–Grant type equation:

$$\dot{\varepsilon}_s t_r \simeq C \tag{9}$$

where C is a constant related to the rupture ductility, ε_r. Thus, the rupture life is correlated with the rupture ductility if the steady-state creep rate, $\dot{\varepsilon}_s$, is the same in the materials referred to. This indicates that the rupture life ratio (t_{rs}/t_{rn}) of the specimen with serrated grain boundaries to the one with straight grain boundaries can also be expressed by a hyperbolic function of the fractal dimension difference between serrated and straight grain boundaries, ΔD. Since the rupture life is generally expressed by a power function of stress, the rupture strength ratio (σ_s/σ_n) of the specimen with serrated grain boundaries to the one with straight grain boundaries can be fitted to a hyperbolic function of the fractal dimension difference, ΔD. Therefore, all the creep-rupture data were fitted to hyperbolic functions of ΔD in this study.

It was also found in the creep-ruptured specimens that the correlation between creep-rupture properties and the fractal dimension of the fracture surface profile was not so good as that between the properties and the fractal dimension of the grain boundary. This may be attributed to several factors such as creep deformation of the grains, grain-boundary migration, and oxidation and surface diffusion at high temperatures.

4. Fractal dimension and fracture mechanism in carbon steels

Fig. 6 shows the creep-rupture properties of carbon steels with ferrite–pearlite structure tested under a stress of 49 MPa at 873 K. The rupture life has a maximum at a pearlite volume fraction of about 0.7, but the rupture ductility decreases with increasing pearlite volume fraction. Fig. 7 shows the fractal dimensions of the ferrite grain boundary, ferrite–pearlite phase boundary, pearlite grain boundary and the fractal dimension of the fracture surface profile in the ferrite–pearlite steels. The fractal dimension of the ferrite–pearlite grain boundary and that of the pearlite grain boundary decrease with increasing pearlite volume fraction, while the fractal dimension of the ferrite grain boundary is much the same in four specimens. This may indicate that the ferrite–pearlite and pearlite–pearlite grain boundaries are somewhat irregular in the relatively early stage of growth of pearlite nodules.

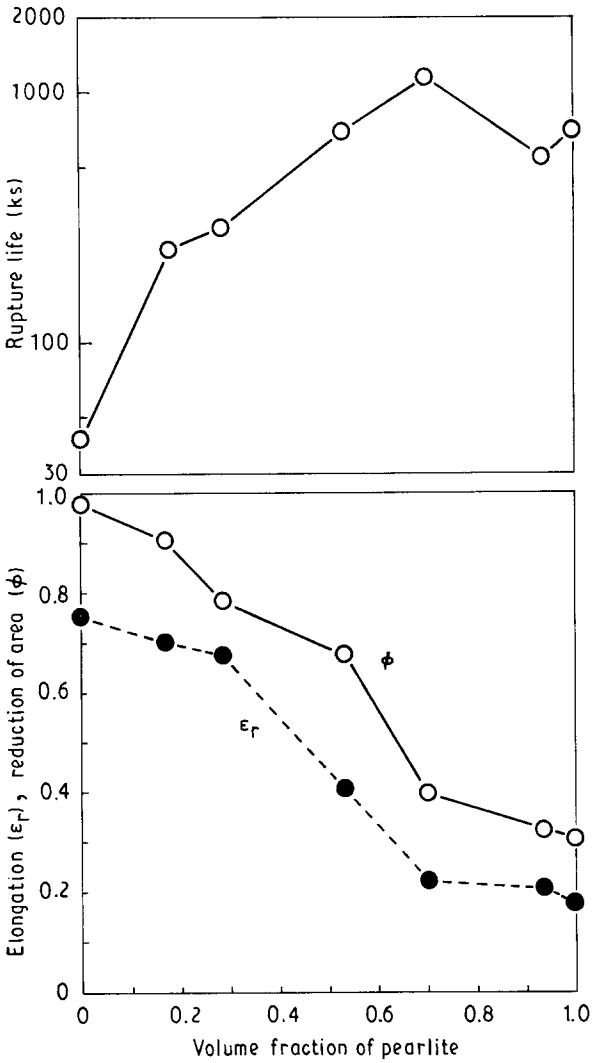

Figure 6 Creep-rupture properties of ferrite–pearlite steels tested under a stress of 49 MPa at 873 K.

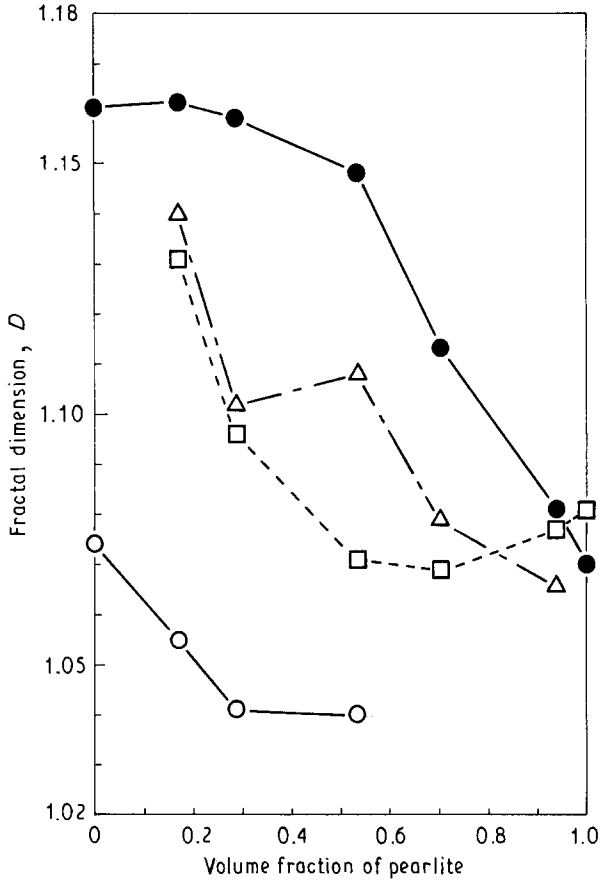

Figure 7 Fractal dimensions of (○) ferrite grain boundary, (△) ferrite–pearlite grain boundary, (□) pearlite grain boundary and (●) fracture surface profile in ferrite–pearlite steels tested under a stress of 49 MPa at 873 K.

The fractal dimension of the fracture surface profile also decreases with increasing pearlite volume fraction. In pure iron and low-carbon steels with a pearlite volume fraction less than 0.286, in which transgranular fracture occurs, the fractal dimension of the fracture surface profile is relatively larger than those of three kinds of grain boundary. In medium-carbon steels with a pearlite volume fraction between 0.532 and 0.701, in which the predominant fracture occurs at ferrite–pearlite grain boundaries, the fractal dimension of the fracture surface profile is close to that of the ferrite–pearlite or pearlite grain boundary, although a little larger value of the former fractal dimension may indicate the importance of creep deformation in the ferrite matrix. In high-carbon steels with a pearlite volume fraction larger than 0.935, the fractal dimension of the fracture surface profile is almost the same as that of the pearlite grain boundary. This indicates that the pearlite grain boundary is the fracture path. Thus, the dominant fracture mechanism can be confirmed from the correlation between the fractal dimension of the fracture surface and that of the grain boundary in ferrite–pearlite steels when grain-boundary fracture occurs.

5. Conclusions

The grain-boundary configuration of heat-treated specimens and the fracture surface roughness of creep-ruptured specimens in heat-resistant alloys were quantitatively evaluated on the basis of fractal geometry. The fractal dimension of the grain boundary and that of the fracture surface profile in these specimens were estimated by using the vertical section method. The relations between the fractal dimension of the grain boundary, that of the fracture surface profile, the creep-rupture properties and the fracture mechanisms of the alloys were then discussed. The methods used to estimate the fractal dimensions of grain boundary and fracture surface profile were also examined. The results obtained are summarized as follows.

1. The grain-boundary configuration in heat-resistant alloys was quantitatively characterized by the fractal dimension of the grain boundary. The fractal dimension of a nominally serrated grain boundary was always larger than that of a straight grain boundary in the same alloy. The relative importance of the ruggedness of grain boundaries was estimated by the fractal dimension difference between these two types of grain boundary. The fractal dimension of the grain boundary increased with the occurrence of grain-boundary precipitates, but prolonged ageing caused the coarsening of precipitates and led to a decrease of the fractal dimension.

2. The fractal dimension of the grain boundary and that of the fracture surface profile were obtained in this study by the method of covering grain boundaries or the centre of grain-boundary precipitates and fracture surface profiles with circles of a given diameter. The method using square grids employed in the previous study gave larger values for the fractal dimension of the grain boundary than the present method.

3. The fractal dimension of the fracture surface profile was correlated with that of the grain boundary when the grain boundary was the fracture path. The fractal dimension of the fracture surface profile was almost the same as that of the grain boundary when the creep ductility of the material was relatively low, but the former value somewhat differed from the latter one when extensive creep deformation in the grains, grain-boundary migration, surface diffusion or oxidation occurred during high-temperature creep.

4. There was a quantitative relationship between the relative increase of the fractal dimension of the grain boundary owing to grain-boundary serration and the increases in creep ductility and rupture life or rupture strength of heat-resistant alloys. The improvement of the rupture life was attributed to an increase of creep ductility, which was correlated with the increased ruggedness and length of serrated grain boundaries. There was also a correlation between the improvement of creep-rupture properties and the increase in the fractal dimension of the fracture surface profile due to grain-boundary serration.

5. In carbon steels with ferrite–pearlite structure creep-ruptured under a stress of 49 MPa at 873 K, according to the increase in pearlite volume fraction, the rupture ductility decreased and the fracture mechanism changed from transgranular fracture in pure iron and low-carbon steels to predominant fracture at ferrite–pearlite grain boundaries in medium-carbon steels, and further to intergranular fracture at pearlite grain boundaries in high-carbon steels. The fractal dimension of the fracture surface profile decreased with the pearlite volume fraction of the steel. The fractal dimension of the fracture surface profile was correlated with the fractal dimension of the ferrite–pearlite grain boundary or that of the pearlite grain boundary when grain-boundary fracture occurred.

References

1. B. B. MANDELBROT, D. E. PASSOJA and A. J. PAULLAY, *Nature* **308** (1984) 721.
2. E. HORNBOGEN, *Z. Metallkde* **78** (1987) 622.
3. B. SPRUŠIL, H. U. FRITSCH and B. L. MORDIKE, *ibid.* **79** (1988) 50.
4. E. HORNBOGEN, *Acta Metall.* **32** (1984) 615.
5. T. KLEISER and M. BOČEK, *Z. Metallkde* **77** (1986) 582.
6. M. YAWORSKI and J. G. BYRNE, *Metall. Trans. A* **19A** (1988) 1371.
7. K. BANERJI, *ibid.* **19A** (1988) 961.
8. C. S. PANDE, L. E. RICHARDS, N. LOUAT, B. D. DEMPSEY and A. J. SCHWOEBLE, *Acta Metall.* **35** (1987) 1633.
9. J. L. CHERMANT and M. COSTER, *J. Mater. Sci.* **14** (1979) 509.
10. M. TANAKA, O. MIYAGAWA, T. SAKAKI, H. IIZUKA, F. ASHIHARA and D. FUJISHIRO, *ibid.* **23** (1988) 621.
11. M. TANAKA, H. IIZUKA and F. ASHIHARA, *ibid.* **23** (1988) 3827.
12. D. McLEAN, *J. Inst. Metals* **85** (1956–57) 468.
13. M. YAMAZAKI, *J. Jpn. Inst. Metals* **30** (1966) 1032.
14. M. KOBAYASHI, O. MIYAGAWA, T. SAGA and D. FUJISHIRO, *J. Iron Steel Inst. Jpn (Tetsu to Hagané)* **58** (1972) 751.
15. M. YAMAMOTO, O. MIYAGAWA, M. KOBAYASHI and D. FUJISHIRO, *ibid.* **63** (1977) 1848.
16. M. TANAKA and H. IIZUKA, in Proceedings of International Conference on Creep, Tokyo, 1986 (Japanese Society for Mechanical Engineering, Tokyo, 1986) p. 187.
17. H. KITAGAWA and R. YUUKI, *Trans. Jpn. Soc. Mech. Eng. Ser. A* **41** (1975) 1641.
18. M. ISHIDA, *ibid.* **45** (1979) 306.
19. S. SURESH, *Metall. Trans. A* **14A** (1983) 2375.
20. M. TANAKA, O. MIYAGAWA, T. SAKAKI and D. FUJISHIRO, *J. Iron Steel Inst. Jpn (Tetsu to Hagané)* **65** (1979) 939.
21. R. RAJ and M. F. ASHBY, *Metall. Trans.* **2** (1971) 1113.
22. M. TANAKA and H. IIZUKA, *Z. Metallkde* **82** (1991) 442.
23. B. B. MANDELBROT, "The Fractal Geometry of Nature", translated by H. Hironaka (Nikkei Science, Tokyo, 1985) p. 25.
24. H. TAKAYASU, "Fractal" (Asakura, Tokyo, 1986) p. 7.
25. M. YOSHIBA, O. MIYAGAWA and D. FUJISHIRO, *J. Iron Steel Inst. Jpn (Tetsu to Hagané)* **68** (1982) 1813.
26. S. ISHIMURA and S. ISHIMURA, "Fractal Mathematics", (Tokyo Book Co., Tokyo, 1990) p. 240.
27. M. TANAKA, H. IIZUKA and M. TAGAMI, *J. Mater. Sci.* **24** (1989) 2421.
28. M. TANAKA and H. IIZUKA, *Z. Metallkde* **81** (1990) 149.

Received 30 April
and accepted 2 August 1991